The Unusual Self-Organization of Dialkyldithiophosphinic Acid Self-Assembled Monolayers on Ultrasmooth Gold

ARTICLE *in* JOURNAL OF THE AMERICAN CHEMICAL SOCIETY · FEBRUARY 2014

Impact Factor: 12.11 · DOI: 10.1021/ja411140j · Source: PubMed

4 AUTHORS, INCLUDING:

Ronan R San Juan
Dalhousie University
7 PUBLICATIONS **672** CITATIONS

SEE PROFILE

Tricia Breen Carmichael
University of Windsor
36 PUBLICATIONS **1,761** CITATIONS

SEE PROFILE

JACS
JOURNAL OF THE AMERICAN CHEMICAL SOCIETY
Article
pubs.acs.org/JACS

The Unusual Self-Organization of Dialkyldithiophosphinic Acid Self-Assembled Monolayers on Ultrasmooth Gold

Michael S. Miller, Ronan R. San Juan, Michael-Anthony Ferrato, and Tricia Breen Carmichael*

Department of Chemistry and Biochemistry, University of Windsor, Windsor, Ontario, Canada N9B 3P4

Supporting Information

ABSTRACT: We report the formation and characterization of self-assembled monolayers (SAMs) of dialkyldithiophosphinic acid adsorbates $[CH_3(CH_2)_n]_2P(S)$-SH (R_2DTPA) (n = 5, 9, 11, 13, 15) on ultrasmooth gold substrates prepared by the template stripping method. The SAMs were characterized using X-ray photoelectron spectroscopy, reflection–absorption infrared spectroscopy, contact angle measurements, lateral force microscopy, and electrochemical impedance spectroscopy. The data show these SAMs exhibit an unusual trend in alkyl chain crystallinity; SAMs formed from adsorbates with short alkyl chains (n = 5) are ordered and crystalline, and the alkyl groups become increasingly disordered and liquidlike as the number of methylene units is increased. This trend is the opposite of the typical behavior exhibited by n-alkanethiolate SAMs, in which the alkyl layer becomes more crystalline and ordered as the alkyl chain length is increased. We discuss four factors that operate together to determine how R_2DTPA self-organize within SAMs on TS gold: (i) adsorbate–substrate interactions; (ii) gold substrate morphology; (iii) lateral van der Waals interactions between alkyl groups; and (iv) steric demands of the alkyl groups. We also present a model for the structures of these SAMs on the basis of consideration of the data and the structural parameters of a model ^{n}Bu$_2$DTPA adsorbate. In this model, interdigitation of short alkyl chains stabilizes a trans-extended, crystalline arrangement and produces an ordered alkyl layer. As the alkyl chain length is increased, the increased steric demands of the alkyl groups lead to liquidlike, disorganized alkyl layers.

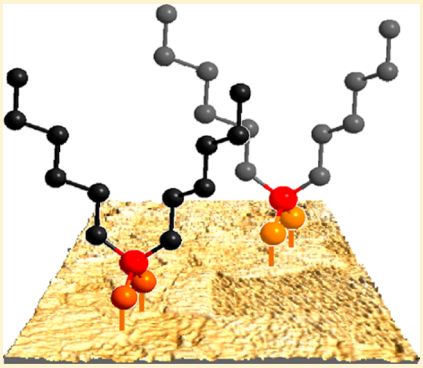

INTRODUCTION

Forming self-assembled monolayers (SAMs) on surfaces is an exceptionally well-studied method to access a wide range of surface properties.[1] After 25 years of research, there have been reported a vast number of SAMs that employ different substrates (metals, metal oxides, semiconductors) and different molecular adsorbates.[2] From these studies, it is generally accepted that two factors—the interaction between the adsorbate headgroup and the substrate, and lateral interactions between the organic portions of the adsorbates—determine the way in which adsorbates self-organize on surfaces to form SAMs. The interplay between these two factors determines structural features such as molecular packing density, molecular tilt, and crystallinity of the alkyl layer of the resulting SAM. These structural features have a practical importance because they contribute to the macroscopic surface properties of the SAM, such as wettability, frictional properties, and the ability of guest molecules to intercalate into the SAM. Predicting the details of SAM structure is fairly straightforward for adsorbates with simple structures, such as n-alkanethiolates. For example, adsorbate–substrate interactions and lateral van der Waals interactions between adsorbates are sufficient to explain the structures of n-alkanethiolate SAMs with different alkyl chain lengths on gold substrates.[3,4] The highly favorable Au–S adsorbate–substrate interaction stabilizes the SAM and determines the maximum packing density of the adsorbates. SAMs formed from n-alkanethiolates with short alkyl chains have liquidlike, disorganized alkyl groups because there are not enough van der Waals interactions possible between adjacent alkyl chains to stabilize a trans-extended, crystalline arrangement. As the number of methylene groups increases, however, the increasing number of van der Waals interactions between alkyl chains causes the progression from a liquidlike organization to one in which the alkyl chains are trans-extended and crystalline. Short-chain, liquidlike SAMs are wet by both water and hexadecane,[4,5] and exhibit higher frictional coefficients than long-chain crystalline SAMs.[5−9] Both properties have been attributed to gauche defects in the short alkyl chains, which expose methylene groups at the surface that contact probe liquids or AFM probe tips. In contrast, crystalline SAMs present a layer of well-packed methyl groups at the surface, causing higher water and hexadecane contact angles and lower frictional forces.

Although predicting the structure of a SAM is fairly straightforward for structurally simple adsorbates, a more rigorous understanding of the interplay between the factors affecting adsorbate self-organization will be necessary to develop design rules to enable the design of adsorbates that produce complex self-organized structures and to predict

Received: October 31, 2013
Published: February 21, 2014

dx.doi.org/10.1021/ja411140j | J. Am. Chem. Soc. 2014, 136, 4212−4222

structures of SAMs formed from structurally complex adsorbates. The ability to design adsorbates that form SAMs with specific structures and adsorbate packing densities is a powerful tool for many applications, such as the design of SAMs to act as sensors that can detect analytes based on shape and functionality with high selectivity.[10] In the field of molecular electronics, there is great interest in studying the charge transport properties of SAMs formed from complex adsorbates in molecular junctions.[11] Complex adsorbates with conjugated backbones, chelating headgroups, or specific functional groups may give rise to useful electronic properties, such as improved coupling to the metal electrodes and rectification.[12−19] Understanding and predicting how these adsorbates self-organize on the surface is essential to the development of these SAM-based devices. To fully elucidate the design rules for SAM formation, it is necessary to first deepen our understanding of the relationship between the adsorbate structure and the resulting SAM structure by studying SAMs formed from structurally complex adsorbates. A leading approach has been to vary the structure of the sulfur-containing headgroup. Studies of bidentate[20−25] and tridentate[26−32] thiols, dithiocarboxylic acids,[33−35] xanthic acids,[36,37] and dialkyldithiocarbamates[12,14,38−41] have all produced SAMs with structures that differ in some way from archetypical *n*-alkanethiolate SAMs. For example, Lee et al. have reported the use of bulky chelating spiroalkanedithiol and trithiol headgroups that enforce spacing between adjacent alkyl substituents.[5,6,9,26,30,42−45] The resulting SAMs exhibit alkyl group packing densities that depend on the combination of the chelating headgroup and pendant alkyl chain lengths. With such adsorbates, it is possible to form SAMs with loosely packed alkyl groups even with long alkyl substituents;[9,30,42] furthermore, these SAMs exhibit enhanced stability to thermal[26] and electrochemical[46] desorption compared to *n*-alkanethiolate SAMs due to the chelate effect. Recent studies of xanthic acid and dithiocarboxylic acid adsorbates reveal subtle structural differences between these SAMs and analogous *n*-alkanethiolate SAMs, indicated by contact angles that exhibit a larger odd−even effect for the former SAMs.[36,47]

Our research group has explored the use of chelating dialkyldithiophosphinic acids $[CH_3(CH_2)_n]_2P(S)SH$ (R_2DTPA) to expand the understanding of the relationship between adsorbate structure and SAM structure, as well as to access SAMs with new structures and interfacial properties.[48−51] One might expect these SAMs to consist of DTPA head groups chelated to the gold substrate as shown in Scheme 1a, and the steric demands of the bulky DTPA headgroup to then space out the alkyl groups and produce SAMs with liquidlike, disorganized alkyl chains. However, a study of SAMs formed from R_2DTPA adsorbates with n = 5, 9, 11, 13, 15 on gold films fabricated by electron beam evaporation (As-Dep gold) showed that these SAMs consist of a 60:40 mixture of chelating and monodentate adsorbates (Scheme 1a and b) regardless of the length of the alkyl substituents, and the organization of the alkyl layer is very similar to that of RSH SAMs.[49,51] R_2DTPA SAMs with short alkyl chains (n = 5, 9) have a liquidlike alkyl layer, and the chains become increasingly ordered and crystalline as the number of methylene groups increases. Through a combination of experimental[49−51] and computational[50] studies, we have determined that, for these SAMs, the interplay between adsorbate−substrate interactions and intermolecular interactions in the SAM does not adequately account for the observed SAM structures. A third factor—the substrate morphology—is an important influence that affects how these adsorbates self-organize. The results of our studies can be summarized by three main points: First, computational studies using a model $(^nBu)_2$DTPA adsorbate show that the energetic difference between monodentate binding and chelation is surprisingly small.[50] Second, even though monodentate binding may be accessible, experimental studies show that it occurs only when provoked by defect sites of the As-Dep gold substrate.[51] As-Dep gold films consist of small (∼25−50 nm) grains separated by deep (∼10 nm) grain boundaries, with a root-mean-squared (RMS) roughness of 2−4 nm.[49,52−55] The constrained spaces of these deep grain boundaries cause R_2DTPA adsorbates to adopt monodentate binding, with chelation likely occurring on the small, atomically flat areas on the tops of the gold grains that measure ∼50 nm across.[49] Support for this idea comes from a study of $(C_{16})_2$DTPA SAMs formed on smooth, template-stripped (TS) gold surfaces, which consist of large, flat gold grains that measure ∼200−500 nm across and are separated by shallow (∼2 nm) grain boundaries.[49,53−56] On TS gold, all $(C_{16})_2$DTPA adsorbates chelate to the surface. The adoption of monodentate binding at grain boundaries of As-Dep gold is believed to impart conformational flexibility to the headgroup, which is necessary for the molecules to bind in these constrained spaces by allowing rotation about the Au−S bond and small changes in the Au−S−P bond angle. Third, the adoption of monodentate binding over chelation is compensated energetically by favorable van der Waals interactions between alkyl groups in the SAM. The conformational flexibility of the monodentate adsorbates enables the alkyl groups to pack densely in R_2DTPA SAMs in on As-Dep gold.[49,51] The resulting van der Waals interactions between alkyl groups, which have been estimated at ∼2 kcal mol^{-1} per methylene unit, compensates for the small energy difference between monodentate binding and chelation, particularly for adsorbates with long alkyl chains. The outcome is that the alkyl layer of R_2DTPA SAMs formed on As-Dep gold becomes progressively more ordered and crystalline as the chain length increases due to the increased number of van der Waals interactions between the chains.[51] In contrast, the alkyl groups of the fully chelated $(C_{16})_2$DTPA SAM on TS gold are loosely packed and disorganized.[49] Having all of the adsorbates anchored to the gold surface at two points restricts the conformational freedom of the headgroup; consequently, the alkyl groups cannot pack together to stabilize a trans-extended, crystalline structure. The result is an alkyl layer that is disordered and liquidlike.

On the basis of studying $(C_{16})_2$DTPA SAMs on TS gold, it is reasonable to suggest that chelation, along with the steric demands of the DTPA headgroup, might limit the packing density in the SAM and that reducing the length of the alkyl

Scheme 1. R_2DTPA Adsorbates Bound to Gold with (a) Chelation and (b) Monodentate Binding

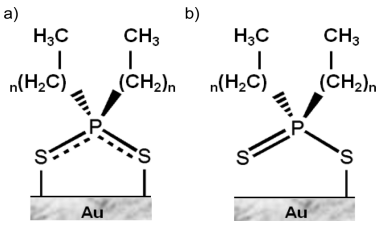

dx.doi.org/10.1021/ja411140j | J. Am. Chem. Soc. 2014, 136, 4212−4222

chain should merely result in a series of SAMs with liquidlike alkyl chains. Here, we present the series of $[CH_3(CH_2)_n]_2$DTPA (n = 5, 9, 11, 13, 15) SAMs on TS gold and show that these SAMs possess structures that exhibit a most surprising trend in alkyl chain crystallinity; SAMs formed from adsorbates with short alkyl chains (n = 5) are ordered and crystalline, and the alkyl groups become increasingly disordered and liquidlike as the number of methylene units is increased. This trend is the opposite of the typical behavior exhibited in n-alkanethiolate SAMs, and it illustrates that changes to the adsorbate structure can have profound and surprising effects on the self-organization of those adsorbates within SAMs. We rationalize the results presented here by considering not only the steric demands and chelation of the headgroup but also the steric demands of the alkyl groups. To our knowledge, R_2DTPA SAMs on TS gold are the first reported example of SAMs with alkyl groups that progress from crystalline to liquidlike as the chain length increases, as well as the first example of SAMs with short (n = 5) alkyl chains that are crystalline.

EXPERIMENTAL SECTION

All chemicals were purchased commercially and used as received. Anhydrous tetrahydrofuran (THF), diethyl ether, and toluene were obtained from an Innovative Technologies solvent purification system. All R_2DTPA molecules were prepared according to published procedures.[49,51] PDMS stamps were prepared by casting PDMS prepolymer against photolithographic masters according to published procedures.[57]

Gold Substrate Preparation. As-Dep gold films were produced by depositing 2 nm titanium as an adhesion promoter followed by 200 nm gold onto silicon wafers using an e-beam evaporator. The gold films were used immediately after their fabrication to form SAMs to minimize surface contamination. TS gold films were prepared according to published procedures.[54] Four hundred nanometers of gold was deposited onto silicon wafers by e-beam evaporation, and then a small drop (10 μL) of Norland Optical Adhesive 83H was applied to the gold surface followed by a 2 cm × 2 cm glass substrate. After curing the adhesive using a UV lamp for 10 min, the glass slide was stripped from the silicon wafer using a scalpel. TS gold films were used immediately after their fabrication for SAM formation to minimize surface contamination.

SAM Formation. Approximately 2 cm × 2 cm As-Dep and TS gold substrates were immersed into a 1 mM R_2DTPA solution in anhydrous toluene or a 1 mM solution of 1-hexadecanethiol in anhydrous ethanol for 24 h. Substrates were then removed from solution, rinsed with anhydrous toluene (for R_2DTPA SAMs) or anhydrous ethanol (for 1-hexadecanethiolate SAMs), and dried under a stream of nitrogen.

Sample Preparation for Lateral Force Microscopy. Microcontact printing of 1-hexadecanethiol onto As-Dep and TS gold substrates was carried out according to published procedures using a PDMS stamp bearing 10-μm-wide raised lines separated by 10-μm-wide recesses.[57] Printed gold substrates were rinsed with anhydrous ethanol, dried using a stream of nitrogen, and placed into a 2 mM toluene solution of R_2DTPA for 15 min. Substrates were removed from the solution, rinsed with anhydrous toluene and anhydrous ethanol, and dried under a stream of nitrogen.

Atomic Force Microscopy (AFM) and Lateral Force Microscopy (LFM). AFM and LFM images were obtained using a Digital Instruments Multimode atomic force microscope run in contact mode. Veeco-type SNL (silicon-tip on nitride lever) cantilevers were used with a nominal tip radius of 2 nm and a nominal force constant of 0.12 N/m. The back side of the cantilever was coated with 45 ± 5 nm of Ti/Au. LFM images were collected over a 75 μm × 75 μm scan area using a scan rate of 1.0 Hz, a scanning resolution of 512 samples/line, and a constant force estimated to be ~0.1 nN. AFM images were collected over a 1 μm × 1 μm scan area using a scan rate of 1.0 Hz and a scanning resolution of 512 samples/line. All images were collected using Nanoscope 6 software, and processed using WSxM 5.0 Develop 1.0 software.[58]

X-ray Photoelectron Spectroscopy (XPS). XPS spectra were collected at Surface Science Western (London, Ontario, Canada) using a Kratos Axis Nova X-ray photoelectron spectrometer with a monochromatic Al Kα source. The detection limit of the instrument is 0.1−0.5 atomic percent. Both survey scan and high-resolution analyses were carried out over a 300 μm × 700 μm scan area. Survey scan analyses were carried out with a pass energy of 160 eV, and high-resolution analyses were carried out with a pass energy of 20 eV. Samples were analyzed at a 30° takeoff angle (60° tilt). High-resolution sulfur line shapes were fit using one pair of spin−orbit-split components (2 $p_{3/2}$ and 2 $p_{1/2}$) assuming a Gaussian:Lorentzian (70%:30%) line shape and a fixed splitting energy of 1.18 eV with a 2:1 area ratio.[59]

Infrared Spectroscopy. Reflection−absorption infrared (RAIR) spectra were collected using a Bruker IFS 66/v spectrometer equipped with an MCT detector and Harrick Autoseagull accessory. The p-polarized light was incident at 85° from the surface normal; 1024 scans were collected at a resolution of 2 cm^{-1}.

Contact Angle Measurements. Water and hexadecane contact angles were measured using the sessile drop method on a Rame-Hart contact angle goniometer equipped with a microliter syringe and a tilting stage. In each case, at least three drops from three samples (i.e., at least nine independent measurements) were averaged.

Electrochemical Impedance Spectroscopy (EIS). EIS spectra were collected using a BAS-Zahner IM6 ex-impedance unit. A glass cell equipped with a calomel/saturated KCl reference electrode and a 1.0 mm Pt wire counter electrode was clamped to the working electrode, a 0.95-cm^2 area of the SAM on gold, and then filled with an aqueous solution of 1 mM $K_3Fe(CN)_6$, 1 mM $K_4Fe(CN)_6{\cdot}3H_2O$ and 10 mM Na_2SO_4. The measurements were made at an open circuit potential set at 450 mV with a 5 mV ac perturbation that was controlled from 5.0 × 10^{-2} to 2.0 × 10^5 Hz. SAM resistance and capacitance values were normalized to the area of the working electrode.

RESULTS AND DISCUSSION

Gold Substrate and R_2DTPA SAM Preparation. We fabricated TS gold substrates by e-beam evaporation of 400 nm of gold onto a silicon wafer, followed by adhering a 2 cm × 2 cm glass slide on the surface using an optical adhesive. After curing the adhesive, we removed the glass slide using a scalpel to expose the smooth underside of the film. These substrates consist of grains with sizes ranging from 200 to 500 nm with grain boundaries that are ~2 nm deep, and a root-mean-square roughness of 0.5 nm (Figure 1). We synthesized R_2DTPA compounds according to published procedures,[49,51] and prepared SAMs by immersing TS gold substrates into 1 mM solutions of each adsorbate in toluene for 24 h.

Binding of the DTPA Head Group to the Gold Surface. X-ray photoelectron spectroscopy (XPS) revealed that both sulfur atoms of R_2DTPA adsorbates interact with the TS gold surface, indicating that the SAMs contain only chelating

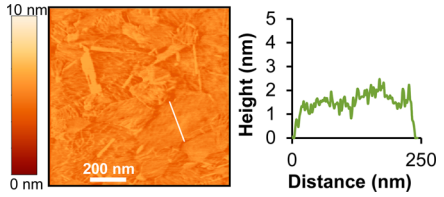

Figure 1. AFM topographic image recorded in contact mode of a typical TS gold film. The white line shows the region that corresponds to the cross-sectional profile depicted beside the image.

dx.doi.org/10.1021/ja411140j | J. Am. Chem. Soc. 2014, 136, 4212−4222

adsorbates regardless of the alkyl chain length. Survey scans of R_2DTPA SAMs formed on TS gold (Figure S1 in Supporting Information [SI]) showed characteristic binding energies of gold, as well as the elements comprising the R_2DTPA adsorbates (P, S, C). Survey scans also showed the presence of oxygen. We used high-resolution XPS (HR-XPS) of the S 2p region to determine the binding state of the DTPA adsorbates to the gold surface. The electronic environment of the sulfur atom and the nature of the interaction between sulfur and gold surface atoms influence the S 2p binding energies. Previous HR-XPS studies of sulfur-containing SAMs on gold have established that the S $2p_{3/2}$ peaks of sulfur atoms bound to gold appear at binding energies of ~161−162 eV, whereas sulfur atoms that are not interacting with the gold surface give S $2p_{3/2}$ peaks at binding energies of ~163−165 eV, and oxidized sulfur species give S $2p_{3/2}$ peaks at binding energies >166 eV.[60,61] HR-XPS of the S 2p region of R_2DTPA SAMs on TS gold (Figure 2) showed a simple line shape that we fit using one pair of

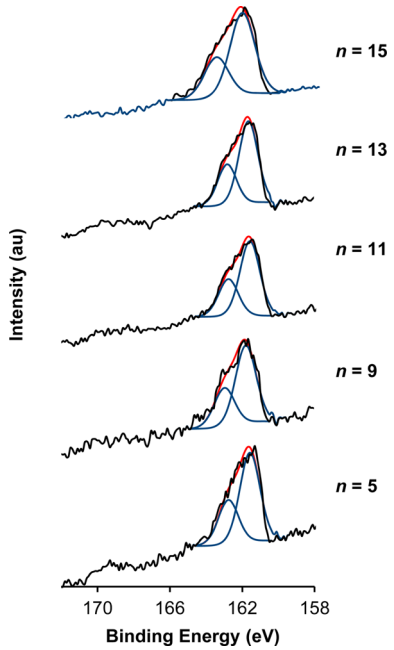

Figure 2. HR-XPS spectra of the S 2p region for $[CH_3(CH_2)_n]_2$DTPA SAMs on TS gold.

spin−orbit-split components (S $2p_{3/2}$ and S $2p_{1/2}$) by assuming a Gaussian/Lorentzian (70%:30%) line shape and a splitting energy fixed at 1.18 eV.[59] The fitted data show S $2p_{3/2}$ peaks at binding energies ~161−162 eV (Table 1), which indicate that

Table 1. S $2p_{3/2}$ Binding Energies of $[CH_3(CH_2)_n]_2$DTPA SAMs on TS gold

	$[CH_3(CH_2)_n]_2$DTPA SAM				
	n = 5	n = 9	n = 11	n = 13	n = 15
S $2p_{3/2}$ binding energy (eV)	161.6	161.7	161.6	161.6	161.5

all sulfur atoms in these SAMs are bound to the gold substrate. Accordingly, all of the adsorbates are chelated to the gold surface, regardless of the alkyl chain length.

HR-XPS spectra of the S 2p region furthermore show that the oxygen detected in survey scans of R_2DTPA SAMs on TS gold is likely due to the adsorption of adventitious oxygen-containing species rather than oxidation of the DTPA headgroup. The absence of peaks at binding energies >168 eV, which correspond to oxidized sulfur species, is consistent with protection of the DTPA sulfur atoms from oxidation even for the shortest alkyl chain lengths studied. In contrast, XPS studies of R_2DTPA SAMs on As-Dep gold with short alkyl chains (hexyl and decyl) show S $2p_{3/2}$ peaks at binding energies >168 eV.[51] In these SAMs, the hexyl and decyl chains are too short and disordered to prevent the penetration of oxygen through the SAM to the headgroup, resulting in DTPA oxidation. On TS gold, chelation of the headgroup and/or differences in alkyl group packing (*vide infra*) likely protect the headgroup from oxidation. Previously reported DTPA SAMs on As-Dep gold with long alkyl chains—R_2DTPA SAMs (n = 11, 13, 15) and R^1R^2DTPA SAMs (R^1 = hexyl, R^2 = decyl, hexadecyl)—do not show peaks in the HR-XPS spectra due to oxidized sulfur species, suggesting that the alkyl groups are long enough in these SAMs to protect the headgroup from oxidation.[48,51] However, survey scans of these SAMs do exhibit peaks due to oxygen, which have been attributed to the adsorption of adventitious species that contain oxygen. The presence of oxygen in the XPS survey scans of R_2DTPA SAMs on TS gold suggests that these SAMs, like their long-chain counterparts on As-Dep gold, do not prevent adsorption of such oxygen-containing species.

Organization of the Alkyl Chains. Reflection absorption infrared spectroscopy (RAIRS) revealed an unexpected trend in the organization of the alkyl layer of R_2DTPA SAMs on TS gold: SAMs with short (n = 5) alkyl chains are highly crystalline, and the layer becomes more disordered and liquidlike as the number of methylene units in the alkyl chain increases. This trend directly counters that of R_2DTPA SAMs on As-Dep gold and RSH SAMs on coinage metals, which exhibit the typical trend of increasing alkyl group crystallinity as the number of methylene units in the chain increases.[3,4,51] The typical trend can be straightforwardly explained by the increasing number of van der Waals interactions between the chains as the chain length increases. We assessed the crystallinity of the alkyl layers of R_2DTPA SAMs on TS gold by examining the frequencies of the asymmetric and symmetric methylene C−H stretching modes, which are diagnostic of alkyl chain crystallinity,[3] and by comparing these peak frequencies to those of RSH SAMs and R_2DTPA SAMs on As-Dep gold. RAIR spectra of the R_2DTPA SAMs on TS gold are shown in Figure 3, along with dotted lines at 2918 cm^{-1} and 2850 cm^{-1} that correspond to the $\nu_{as}(CH_2)$ and $\nu_s(CH_2)$ stretching frequencies for the crystalline chains of C_{16}SH SAMs on gold for comparison. The spectra show that, as expected, the intensities of the $\nu_{as}(CH_2)$ and $\nu_s(CH_2)$ peaks increase as the number of methylene groups increases. At the same time, the $\nu_{as}(CH_2)$ and $\nu_s(CH_2)$ peak frequencies also increase, which corresponds to a decrease in chain crystallinity. The SAM with the shortest alkyl chain length, $(C_6)_2$DTPA, exhibits the highest crystallinity, with $\nu_{as}(CH_2)$ and $\nu_s(CH_2)$ stretching frequencies of 2919 cm^{-1} and 2850 cm^{-1}, respectively, that are nearly identical to C_{16}SH SAMs on gold and $(C_{16})_2$DTPA SAMs on As-Dep gold (Table 2). Increasing the chain length of the R_2DTPA SAM from hexyl to decyl increases the $\nu_{as}(CH_2)$ stretching frequency by 3 cm^{-1} (Table S1 in SI). It has previously been reported that the $\nu_{as}(CH_2)$ stretching frequency is highly sensitive to small changes in conformational order for highly ordered SAMs.[45] Thus, the 3 cm^{-1} difference between the asymmetric C−H stretching frequencies of

dx.doi.org/10.1021/ja411140j | J. Am. Chem. Soc. 2014, 136, 4212−4222

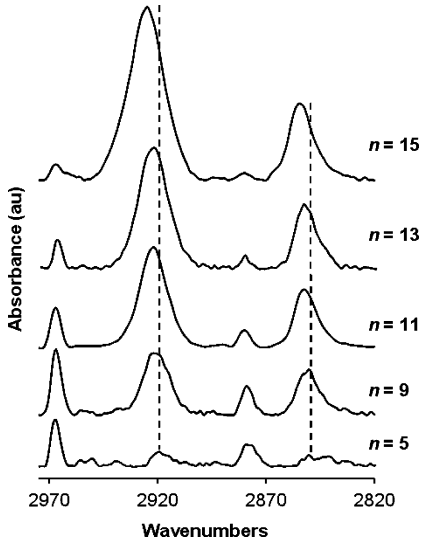

Figure 3. RAIR spectra (2970 - 2820 cm^{-1}) of $[CH_3(CH_2)_n]_2$DTPA (n = 5, 9, 11, 13, 15) SAMs formed on TS gold. Dashed lines correspond to symmetric (2850 cm^{-1}) and asymmetric (2918 cm^{-1}) methylene C−H stretches of C_{16}SH SAMs formed on TS gold.

Table 2. Comparison of Asymmetric and Symmetric Methylene C−H Stretching Frequencies for R_2DTPA (n = 5, 15) SAMs on TS gold, RSH (n = 5, 15) SAMs on TS gold, and R_2DTPA (n = 5, 15) SAMs on As-Dep gold

	peak positions (cm^{-1})			
	n = 5		n = 15	
SAM	$\nu_{as}(CH_2)$	$\nu_s(CH_2)$	$\nu_{as}(CH_2)$	$\nu_s(CH_2)$
$[CH_3(CH_2)_n]_2$DTPA on TS Au	2919	2850	2925	2854
$CH_3(CH_2)_n$SH on TS Au	2921	2852	2917	2850
$[CH_3(CH_2)_n]_2$DTPAon As-Dep Au[a]	2922	2853	2918	2850

[a]Peak positions of R_2DTPA SAMs on As-Dep gold obtained from reference 48.

$(C_6)_2$DTPA and $(C_{10})_2$DTPA SAMs is meaningful, indicating that hexyl chains are more ordered than decyl chains. The chains then become increasingly disordered as the alkyl chain length is further increased. The SAM with the longest chain length, $(C_{16})_2$DTPA, exhibits the most disorder, with $\nu_{as}(CH_2)$ and $\nu_s(CH_2)$ stretching frequencies at 2925 cm^{-1} and 2854 cm^{-1}, indicative of a SAM in which the alkyl layer is more disordered and liquidlike than even C_6SH SAMs on gold and $(C_6)_2$DTPA SAMs on As-Dep gold (Table 2).

As the alkyl chain length of R_2DTPA SAMs on TS gold increases and the chains become more liquidlike, the orientation of the methyl groups also becomes more heterogeneous. Analysis of the asymmetric methyl C−H stretches at ~2967 cm^{-1} indicates that these peaks become broader as the length of the alkyl chain increases (Figure 3). The uniformity of the orientation of the methyl groups influences the breadth of the asymmetric methyl stretch. Methyl groups of crystalline SAMs are tightly packed and uniformly oriented, which produces sharp $\nu_{as}(CH_3)$ peaks, whereas the disordered methyl groups of liquidlike SAMs are heterogeneously oriented and produce broad $\nu_{as}(CH_3)$ peaks.[40] As the alkyl chain length increases, the full width at half-maximum (fwhm) of the $\nu_{as}(CH_3)$ peak of R_2DTPA SAMs on TS gold increases from 5.0 cm^{-1} for the $(C_6)_2$DTPA SAM to 6.5 cm^{-1} for the $(C_{16})_2$DTPA SAM (Table S1 in SI). The narrower width of the $\nu_{as}(CH_3)$ peak of the $(C_6)_2$DTPA SAM compared to the $(C_{16})_2$DTPA SAM is consistent with crystalline, uniformly oriented alkyl chains in the former SAM and liquidlike, disorganized alkyl chains in the latter SAM.

To explain the unexpected trend in alkyl chain crystallinity observed for R_2DTPA SAMs on TS gold, we must understand the factors that control how the adsorbates self-organize on the TS gold surface. We have previously reported that the packing density of the alkyl chains of $(C_{16})_2$DTPA SAMs formed on As-Dep and TS gold depends on how the adsorbates in the SAM bind to the gold substrate.[49] On As-Dep gold, the conformational flexibility of the monodentate $(C_{16})_2$DTPA adsorbates enables dense packing of the alkyl groups and, consequently, the interchain van der Waals interactions that stabilize a trans-extended, crystalline alkyl layer. In contrast, the liquidlike alkyl chains of $(C_{16})_2$DTPA SAMs on TS gold indicate that there is a difference in how these adsorbates pack in the SAM. On the basis of this study, we concluded that, because all adsorbates chelate on TS gold, the inflexibility of the chelated head groups, along with the steric demands of the bulky DTPA headgroup, likely reduces the packing density of these adsorbates on the surface compared to $(C_{16})_2$DTPA SAMs on As-Dep gold. Reduced adsorbate packing density consequently limits the interchain van der Waals interactions necessary to stabilize trans-extended and crystalline alkyl groups, and instead leads to a disordered alkyl layer. The present study shows that this conclusion is only part of the picture; reducing the steric demands of the alkyl groups by shortening the chain length profoundly changes the structures of R_2DTPA SAMs on TS gold. The alkyl layer becomes increasingly crystalline as the steric demands of the alkyl group are decreased, which may signify that the packing density of the adsorbates in the SAM also changes. We quantitatively determined packing densities of the series of R_2DTPA SAMs on TS gold by calculating the atomic ratios of sulfur to gold (S/Au) for each SAM from the XPS spectra (Table 3). We also normalized these ratios to the packing density of the $(C_{16})_2$DTPA SAM on As-Dep gold, and include the packing densities expressed as percentages in Table 3. As expected, every SAM on TS gold is less densely packed than the $(C_{16})_2$DTPA SAM on As-Dep gold, which is consistent with our previous conclusion that bidentate binding reduces the packing density. R_2DTPA SAMs on TS gold with

Table 3. XPS data for R_2DTPA (n = 5, 15) SAMs on TS gold and $(C_{16})_2$DTPA SAM on As-Dep gold with relative packing densities

	integrated XPS peak area			
SAM	Au 4f	S 2p	S/Au	relative molecular packing density (%)
$(C_{16})_2$DTPA (As-Dep Au)	71406	774	0.011	100
$(C_6)_2$DTPA (TS Au)	87404	483	0.0055	50
$(C_{10})_2$DTPA (TS Au)	79273	642	0.0081	75
$(C_{12})_2$DTPA (TS Au)	85462	662	0.0078	72
$(C_{14})_2$DTPA (TS Au)	86686	659	0.0076	70
$(C_{16})_2$DTPA (TS Au)	79521	658	0.0083	76

dx.doi.org/10.1021/ja411140j | J. Am. Chem. Soc. 2014, 136, 4212−4222

chain lengths from decyl to hexadecyl have similar packing densities ranging from 70 to 76%. Surprisingly, the packing density of the $(C_6)_2$DTPA SAM is markedly low (50%). The $(C_6)_2$DTPA SAM on TS gold thus possesses rather contradictory attributes: the alkyl chains are the most crystalline, yet the adsorbates have the lowest packing density.

To rationalize the unexpected results for the $(C_6)_2$DTPA SAM, we consider how the molecules can self-organize on the surface to produce alkyl chains that are crystalline. Although a definitive answer to this question is beyond the scope of this paper and will likely require careful study using scanning tunneling microscopy, we present a plausible scenario based on the van der Waals distances between alkyl chains necessary to stabilize a trans-extended, crystalline arrangement along with the geometric parameters previously calculated for a model $(^nBu)_2$DTPA adsorbate.[50] In RSH SAMs on gold, the S···S distance between adjacent adsorbates (4.97 Å) is too large to allow van der Waals interactions between adjacent alkyl groups; consequently, the adsorbates tilt about 30° to reduce the distance between adjacent methylene groups to 4.2 Å, which enables interchain van der Waals interactions and produces a crystalline alkyl layer.[1] The alkyl groups of adjacent DTPA adsorbates from the viewpoint in Scheme 2a are also too far apart to stabilize crystalline chains. In Scheme 2a, we consider the distance between the C−P−C planes of adjacent adsorbates. Even when the adsorbates are brought unrealistically close (making the S···S distance 2 Å, which corresponds to the S−S bond length in a dialkyldisulfide),[63] the distance between adjacent C−P−C planes is 5 Å.[64] On the other hand, we can also consider adjacent DTPA adsorbates from the viewpoint depicted in Scheme 2b, in which the alkyl chains are directed toward one another. These chains can interact with one another if they interdigitate. For the $(C_6)_2$DTPA SAM, this configuration may enable sufficient interchain van der Waals interactions to stabilize chain crystallinity. Interdigitation would also produce a rather porous alkyl layer, which is supported by experimental evidence derived from contact angle measurements, lateral force microscopy (LFM), and electrochemical impedance spectroscopy (EIS) (*vide infra*). As the chain length increases, however, the increased space necessary for trans-extended, interdigitated alkyl chains would likely reduce the packing density of adsorbates in the SAM, sacrificing the formation of highly favorable Au−S bonds. We propose that for chain lengths >hexyl, van der Waals interactions between trans-extended alkyl groups are not enough to compensate for the reduction in Au−S bonds. For these chain lengths, the two processes that stabilize the SAM—the formation of favorable Au−S bonds and interchain van der Waals forces via interdigitation—are at odds with each other, in contrast to RSH SAMs where these forces work in concert to stabilize the SAM. It is energetically more favorable to sacrifice trans-extended and ordered chains in favor of increasing the number of Au−S bonds; as a result, R_2DTPA SAMs with long alkyl chains have adsorbates that pack as densely as possible, with alkyl layers that become increasingly disorganized and liquidlike as the chain length increases. The $(C_6)_2$DTPA SAM is thus a special case, in which the short alkyl chains can self-organize in such a way that van der Waals interactions between trans-extended alkyl chains energetically compensate for a lower packing density.

Contact angles of hexadecane (HD) on R_2DTPA SAMs on TS gold are consistent with the proposed model. The contact angle data of R_2DTPA SAMs on TS gold are plotted as a function of the number of methylene groups in the alkyl chains in Figure 4a and tabulated in Table S3 in SI. We also include contact angle data of R_2DTPA SAMs on As-Dep gold as a comparison system that follows the typical trend of increasing

Scheme 2. Diagrams Depicting Two Possibilities for the Self-Organization of $(C_6)_2$DTPA Adsorbates in SAMs on TS gold; (a) $(C_6)_2$DTPA Adsorbates Aligned Laterally and (b) $(C_6)_2$DTPA Adsorbates Oriented to Enable Interdigitation of the Alkyl Chains

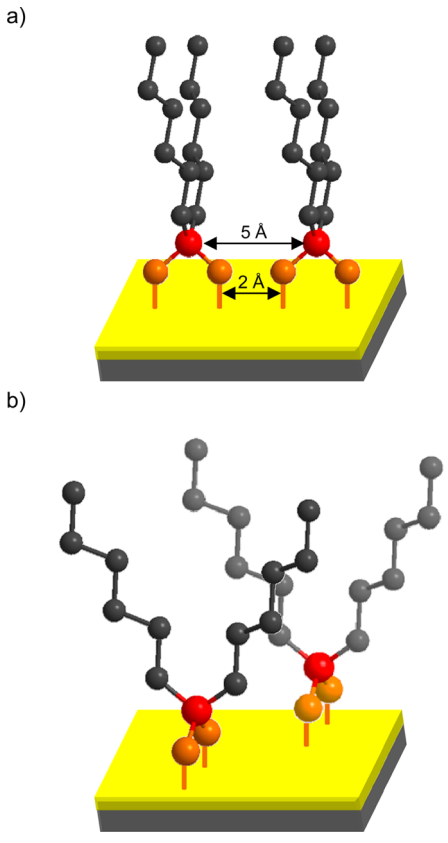

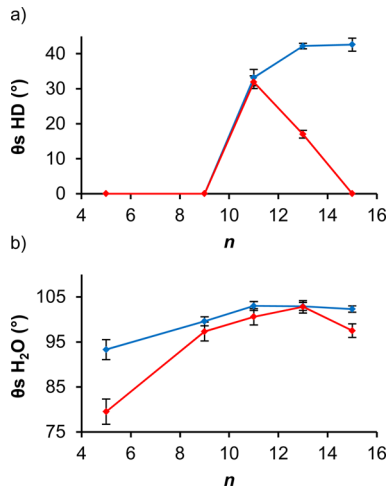

Figure 4. Hexadecane (a) and water (b) contact angles of R_2DTPA (n = 5, 9, 11, 13, 15) SAMs on TS gold (red) and As-Dep gold (blue) plotted as a function of the number of methylene groups in the alkyl chains.

dx.doi.org/10.1021/ja411140j | J. Am. Chem. Soc. 2014, 136, 4212−4222

alkyl chain crystallinity as a function of chain length. HD is a low surface tension liquid that is sensitive to the structure and density of the alkyl chains of SAMs.[4,65,66] HD contact angles are typically low on SAMs with liquidlike alkyl groups due to interactions with exposed methylene groups. On SAMs formed from adsorbates with short alkyl chains, such as C_6SH, low HD contact angles can also be caused by interactions between HD and the underlying gold.[4] In contrast, SAMs with long crystalline alkyl chains, such as SAMs of $C_{16}SH$, have a densely packed methyl surface that generates HD contact angles of >40°. HD wets the surfaces of $(C_6)_2$DTPA and $(C_{10})_2$DTPA SAMs on both TS gold and As-Dep gold (contact angle <15°). Although RAIRS data indicate that the alkyl chains are ordered on the former substrate and liquidlike on the latter (Tables S1 and S2 in SI), these SAMs may be too thin to prevent HD from sensing the underlying gold. In addition, both SAMs may expose methylene groups at the surface, either due to the liquidlike, disorganized chains in the SAMs on As-Dep gold or to the interdigitated alkyl groups proposed for SAMs on TS gold. The HD contact angle increases to ~32° on both TS and As-Dep gold when the length of the alkyl chain is increased to $(C_{12})_2$DTPA, suggesting that the alkyl layers of these SAMs are thick enough to screen the underlying gold surface from the HD drop. On both substrates, the contact angles of <40° indicate that the HD drop interacts with methylene units of the alkyl chains, which is consistent with the liquidlike alkyl chains indicated by the $\nu_{as}(CH_2)$ and $\nu_s(CH_2)$ stretching frequencies from RAIRS spectra of $(C_{12})_2$DTPA SAMs on both As-Dep and TS gold (Tables S2 and S3 of SI). On As-Dep gold, the dodecyl chains are not yet long enough to stabilize crystalline packing via interchain van der Waals interactions. Conversely, on TS gold, the dodecyl chains are likely too long to permit the interdigitated packing proposed for alkyl chain crystallinity. As the alkyl chain length is increased further, the HD contact angles sharply diverge: On As-Dep gold, the HD contact angle continues to increase due to the increasing number of interchain van der Waals interactions that impart crystallinity to the alkyl layer, ultimately leading to a well-packed methyl surface. In contrast, on TS gold the HD contact angle decreases to 17° for $(C_{14})_2$DTPA SAM and then wets the surface of the $(C_{16})_2$DTPA SAM. This progression in HD contact angles follows the trend indicated by RAIRS analysis; as the alkyl chain length is increased, the alkyl layer becomes increasingly disordered, exposing more methylene groups that interact with the HD probe liquid and lower the contact angle.

Water contact angle measurements are less sensitive than HD to subtle structural differences between SAMs, such as disorder in the alkyl layer; however, the higher surface tension of water can also yield measurable contact angles on SAMs that are simply wet by HD to provide additional insight into the SAM structure. The water contact angles of $(C_{10})_2$–, $(C_{12})_2$–, $(C_{14})_2$–, and $(C_{16})_2$DTPA SAMs on both TS and As-Dep gold fall within a fairly narrow range (97–103°) (Figure 3b). On these SAMs, the water drop does not distinguish the structural differences implied by RAIRS and HD contact angle measurements. The water contact angles of $(C_6)_2$DTPA SAMs on TS and As-Dep gold, however, are more informative. On TS gold, $\theta_a(H_2O)$ is 80°, whereas on As-Dep gold the value is 93°. This marked difference in water contact angles must stem from the structural differences between $(C_6)_2$DTPA SAMs on TS and As-Dep gold indicated by RAIRS. On As-Dep gold, the water contact angle is similar to that of a C_6SH SAM on gold and is consistent with the short, liquidlike alkyl chains of both SAMs. On TS gold, however, the alkyl chains are crystalline, and yet the contact angle is 13° lower. Generally, SAMs with crystalline alkyl chains present well-packed methyl surfaces that produce water contact angles >100°. The incongruity between chain crystallinity and water contact angle in the $(C_6)_2$DTPA SAM on TS gold can be rationalized by considering the proposed model for this SAM, in which the crystallinity of the alkyl chains is stabilized by an interdigitated arrangement of alkyl chains. Interdigitation likely leads to a porous (but crystalline) alkyl layer that presents a higher density of exposed methylene units than that of the liquidlike alkyl chains of the $(C_6)_2$DTPA SAM on As-Dep gold. A porous alkyl layer may also allow water to penetrate the SAM and interact with the underlying gold substrate.

Frictional Properties. We used lateral force microscopy (LFM) to probe the outermost surface of R_2DTPA SAMs on TS gold to add to our understanding of the unusual trend in crystallinity as a function of the alkyl chain length indicated by RAIRS and contact angle measurements. LFM records frictional forces between the tip and the sample as the tip is raster scanned across the surface. Due to the lower frictional forces of methyl groups compared to methylene groups, this technique can distinguish between densely packed methyl surfaces, which are typical of SAMs comprising ordered and crystalline alkyl groups, and SAM surfaces with exposed methylene groups due to disordered, liquidlike alkyl chains.[8] We characterized the frictional properties of the series of R_2DTPA SAMs on both TS and As-Dep gold using a $C_{16}SH$ SAM as a standard, well-packed methyl surface *in situ* by preparing the samples according to Scheme 3. We first used

Scheme 3. Process Used to Pattern Alternating Lines of R_2DTPA and $C_{16}SH$ SAMs on TS and As-Dep Gold Substrates

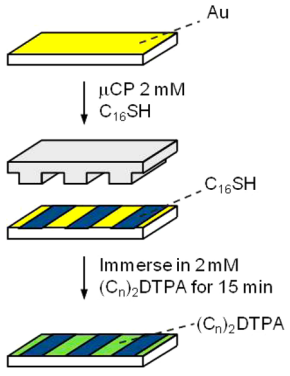

microcontact printing[57] to pattern 10-μm-wide lines of a $C_{16}SH$ SAM onto the gold substrate, and then immersed the substrate into a 2 mM solution of R_2DTPA in anhydrous toluene for 15 min to form a SAM in the 10-μm-wide spaces between the lines of the $C_{16}SH$ SAM. The 15-min exposure time minimizes exchange between R_2DTPA and $C_{16}SH$ molecules, and produces R_2DTPA SAMs that are indistinguishable by RAIRS and XPS from R_2DTPA SAMs formed for 24 h.[49]

LFM images of alternating lines of $C_{16}SH$ and R_2DTPA SAMs on both TS and As-Dep gold are shown in Figure 5. We used a minimal force (~0.1 nN) between the tip and the surface in order to limit penetration of the tip into the SAM. In the resulting LFM images, dark areas correspond to methyl groups (low friction), and bright areas correspond to methylene

dx.doi.org/10.1021/ja411140j | J. Am. Chem. Soc. 2014, 136, 4212–4222

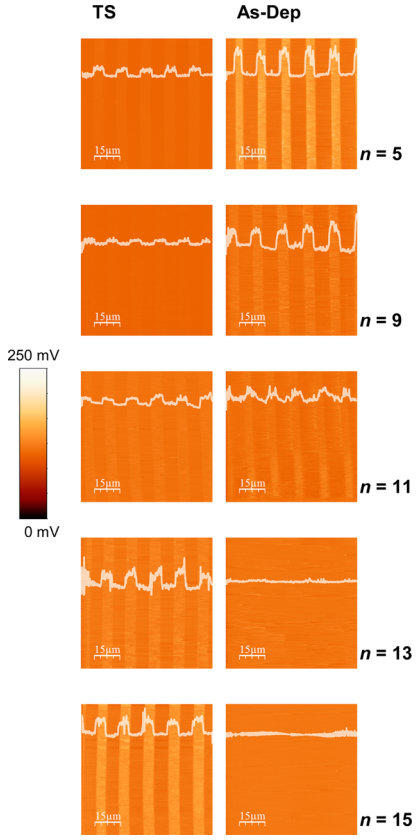

Figure 5. LFM images of alternating lines of $C_{16}SH$ and R_2DTPA (n = 5, 9, 11, 13, 15) SAMs patterned on TS gold (left) and As-Dep gold (right). Bright areas correspond to regions of higher friction. White lines correspond to representative profile measurements depicting the change in friction across the image.

groups (high friction). LFM images of both patterned substrates show a set of lines that are consistently dark, which are due to the well-packed methyl surface of the $C_{16}SH$ SAM. On As-Dep gold, the frictional forces between the tip and the R_2DTPA SAM follow the typical trend: as the alkyl chain length increases, the frictional forces decrease, corresponding to an increase in alkyl group crystallinity and methyl group packing density at the surface. Upon reaching the hexadecyl chain length, the surface of the $(C_{16})_2DTPA$ SAM on As-Dep gold is indistinguishable from that of the $C_{16}SH$ SAM. In contrast, the LFM images of patterned R_2DTPA SAMs on TS gold show that the frictional forces between the tip and the R_2DTPA SAM increase as the alkyl chain length increases, which is consistent with the increasing alkyl group disorder indicated by RAIRS and contact angle measurements. The surface of the $(C_{16})_2DTPA$ SAM exhibits the highest difference in friction compared to the $C_{16}SH$ SAM; not surprisingly, this SAM has the most liquidlike and disorganized alkyl layer of the series according to RAIRS and contact angle data. It is interesting, however, that the frictional forces of the $(C_{10})_2DTPA$ SAM are the lowest (i.e., the most similar to the $C_{16}SH$ SAM) of the series on TS gold, even though RAIRS data indicate that the alkyl chains of the $(C_{10})_2DTPA$ SAM are less crystalline than those of the $(C_6)_2DTPA$ SAM (Table S1 of the SI). At the same time, however, the water contact angle of the $(C_6)_2DTPA$ SAM is 17° lower than that of the $(C_{10})_2DTPA$ SAM. We interpret the markedly low water contact angle of the $(C_6)_2DTPA$ SAM and the slightly higher frictional forces as an outcome of the interdigitated alkyl chains proposed for this SAM; trans-extended, interdigitated alkyl groups may produce a rather porous structure that exposes methylene units to both the water drop and the AFM tip. Increasing the alkyl chain length by four methylene units in the $(C_{10})_2DTPA$ SAM results in an alkyl layer with slightly more disordered chains due to the increased steric demands of these alkyl groups, but the water contact angle increases, and the frictional forces are lower. The methylene groups are evidently screened by the methyl surface in this SAM, which indicates that the structure of this SAM is less porous than that of the $(C_6)_2DTPA$ SAM.

Electrochemical Barrier Properties. We used electrochemical impedance spectroscopy (EIS) to further characterize the structures of R_2DTPA SAMs on TS gold. In the EIS experiment, we applied a small sinusoidal ac perturbation at frequencies ranging from 50 mHz to 20 kHz to the SAM in the presence of an aqueous $K_4Fe(CN)_6/K_3Fe(CN)_6$ redox probe.[67] Measuring the corresponding current response yields the complex impedance of the SAM, which is presented as a Bode magnitude plot for each R_2DTPA SAM on TS gold in Figure 6. We fit the impedance data using a Randles equivalent

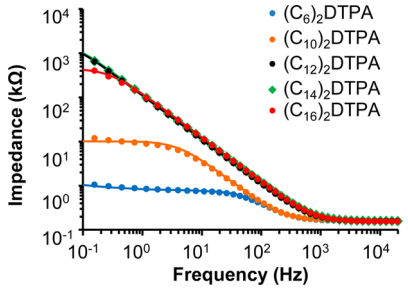

Figure 6. Bode magnitude plots for R_2DTPA SAMs formed on TS gold showing the raw data (dotted lines) and data derived from circuit modeling (solid lines).

circuit to determine values of resistance and capacitance for each SAM. The simple circuit model in Figure 7a was

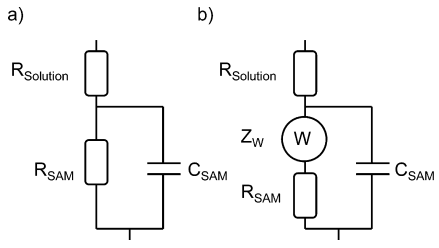

Figure 7. Randles circuit models used to fit raw EIS data of R_2DTPA SAMs on TS gold. (a) Circuit model used to model impedance data of R_2DTPA SAMs with n = 9, 11, 13, 15. (b) Circuit model used to model impedance data of $(C_6)_2DTPA$ SAMs.

appropriate to model the EIS data of R_2DTPA SAMs with alkyl chain lengths ranging from decyl to hexadecyl. This circuit model consists of a solution resistance in series with a parallel Faradaic impedance (R_{SAM}) and coating capacitance (C_{SAM}). The Nyquist plot of the $(C_6)_2DTPA$ SAM (Figure S2 of SI), however, exhibited a 45° Warburg line on the low-frequency side, which indicates that this SAM permits the diffusion of the redox probe molecule through the SAM to the underlying gold.[68] Accordingly, we used the Randles equivalent circuit in

dx.doi.org/10.1021/ja411140j | J. Am. Chem. Soc. 2014, 136, 4212−4222

Figure 7b to model this data. This circuit model includes a Warburg element to model the linear diffusion.

The resistances of R_2DTPA SAMs derived from circuit modeling are plotted in Figure 8a as a function of the number

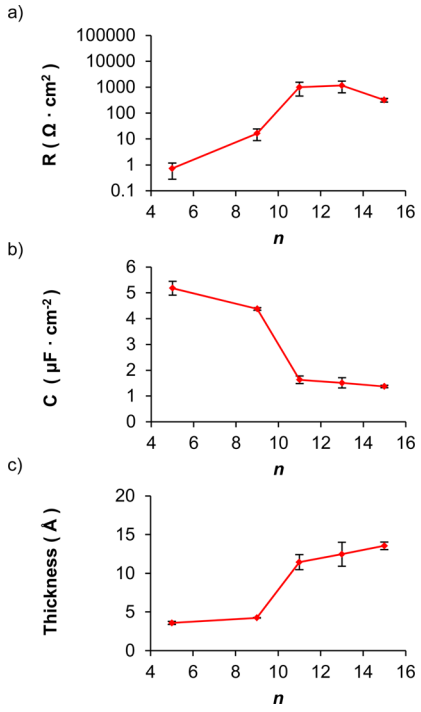

Figure 8. EIS parameters calculated from fitting raw impedance data to the appropriate Randles equivalent circuit model for R_2DTPA (n = 5, 9, 11, 13, 15) SAMs on TS gold. (a) Resistance, (b) capacitance, and (c) thickness plotted as a function of the number of methylene groups in the alkyl chains.

of methylene units in the adsorbate. We used the capacitance values (plotted in Figure 8b) from circuit modeling to calculate SAM thicknesses using the following relation:[3]

$$d = \frac{\varepsilon\varepsilon_0}{C}$$

where d is the SAM thickness in Å, C is the capacitance per area in F m^{-2}, ε is the dielectric constant of the SAM (measured for C_nSH SAMs (n = 16, 18) on gold using surface plasmon resonance to be 2.1),[69] and ε_0 is the permittivity of free space (8.854×10^{-12} F m^{-1}). Capacitances and calculated thickness values of R_2DTPA SAMs are plotted as a function of the number of methylene groups in b and c of Figure 8. Resistance values, capacitances, and calculated thicknesses are tabulated in Table S4 of SI. Among the series of R_2DTPA SAMs studied, the $(C_6)_2$DTPA SAM is unique; despite having alkyl chains with the highest crystallinity, it exhibits the lowest resistance to charge transfer, it is the thinnest SAM, and it is the only one that permits diffusion of the redox probe through the SAM to the gold surface. We have proposed a model for this SAM on the basis of RAIRS, contact angle, and LFM results in which the alkyl layer is porous due to an interdigitated arrangement of crystalline alkyl chains. The barrier properties are consistent with this model, and indicate that the alkyl layer is porous enough to permit diffusion of the redox probe through the SAM. Increasing the chain length to decyl increases the resistance of the SAM by an order of magnitude and reduces diffusion of the redox probe molecule through the SAM, which indicates that this SAM is less porous than the $(C_6)_2$DTPA SAM. Considering these barrier properties along with our interpretation of RAIRS and contact angle data, we conclude that the decyl chains are too long to support the interdigitated, crystalline arrangement proposed for the $(C_6)_2$DTPA SAM; consequently, the packing density increases and the decyl chains become disordered, which lowers the porosity of the alkyl layer and thus prevents diffusion of the redox probe molecule. Despite the addition of four methylene units, the $(C_{10})_2$DTPA SAM is only ~1 Å thicker than the $(C_6)_2$DTPA SAM, which may be due to the change from trans-extended alkyl chains in the $(C_6)_2$DTPA SAM to disordered alkyl chains with gauche defects in the $(C_{10})_2$DTPA SAM. Alkyl chain lengths from dodecyl to hexadecyl form a distinct regime according to the EIS data. These SAMs are thicker and have a higher resistance than SAMs with hexyl and decyl chains; however, they have relatively similar thickness and resistance despite the difference in chain length of four methylene units. RAIRS data indicate that the alkyl groups at these chain lengths are disorganized and liquidlike. Since the alkyl chains in this regime are not trans extended, changing the chain length has a minimal impact on resistance and thickness.

CONCLUSIONS

Identifying the factors that influence the self-assembly of adsorbates on surfaces, and understanding the interplay between them, is essential for the development of design rules to permit the design of adsorbates to produce complex self-organized structures on surfaces. For example, effective design rules may permit the design of adsorbates to produce SAMs with specific adsorbate packing densities, wettabilities, and frictional properties. Surfaces might be custom designed to permit intercalation of specific guest molecules. Our work on SAMs formed from DTPA adsorbates demonstrates that the simplistic picture invoked for *n*-alkanethiolate SAMs on gold, in which adsorbate−substrate interactions and intermolecular van der Waals interactions govern SAM structure, is not sufficient to explain the self-organization of these complex adsorbates on surfaces. The study presented here reveals that the structures of R_2DTPA SAMs on TS gold are determined by the interplay of four factors: (i) adsorbate−substrate interactions; (ii) gold substrate morphology; (iii) lateral van der Waals interactions between alkyl groups; and (iv) steric demands of the alkyl groups. The first two factors operate independently of the alkyl chain length. Regardless of the choice of alkyl substituent, highly favorable Au−S interactions between the R_2DTPA adsorbates and gold substrate are a driving force for the formation of the SAMs, and the smooth morphology of the TS gold surface is necessary to enable chelation of the adsorbate headgroups. The establishment of favorable van der Waals interactions between alkyl chains drives R_2DTPA adsorbates with hexyl substituents to self-assemble in an arrangement that likely features interdigitation of the alkyl groups, leading to a crystalline and ordered alkyl layer. As the chain length is increased, however, the final factor—steric demands of the alkyl groups—comes into play. Interdigitated, trans-extended alkyl groups are no longer energetically favorable when the steric demands are increased because this organization would likely require a reduction in packing density and concomitant loss of favorable Au−S bonds. As a result, the alkyl chains become increasingly liquidlike and disorganized, and the adsorbate packing density increases.

dx.doi.org/10.1021/ja411140j | J. Am. Chem. Soc. 2014, 136, 4212−4222

■ ASSOCIATED CONTENT

Supporting Information

XPS survey scans for R_2DTPA SAMs on TS gold (Figure S1), RAIRS peak positions and intensities of methyl and methylene C−H stretches of R_2DTPA SAMs on TS gold (Table S1), RAIRS peak positions of methylene C−H stretches of R_2DTPA SAMs on As-Dep gold (Table S2), static water and hexadecane contact angles of R_2DTPA SAMs on As-Dep and TS gold (Table S3), Nyquist plots of R_2DTPA SAMs on TS gold (Figure S2), EIS parameters for R_2DTPA SAMs on TS gold calculated from Randles equivalent circuit analysis (Table S4). This material is available free of charge via the Internet at http://pubs.acs.org.

■ AUTHOR INFORMATION

Corresponding Author

tbcarmic@uwindsor.ca

Notes

The authors declare no competing financial interest.

■ ACKNOWLEDGMENTS

This research was supported by the National Sciences and Engineering Research Council of Canada (NSERC) and by the Ontario Ministry of Research and Innovation through an Early Researcher Award to T.B.C. M.S.M. is grateful for the award of an NSERC postgraduate doctoral scholarship. R.R.S. is grateful for the award of an Ontario Graduate Scholarship (OGS). M.-A.F. is grateful for the award of an NSERC summer research fellowship. We thank Mark Biesinger at Surface Science Western for X-ray photoelectron spectroscopy.

■ REFERENCES

(1) Love, C. J.; Estroff, L. A.; Kriebel, J. K.; Nuzzo, R. G.; Whitesides, G. M. *Chem. Rev.* **2005**, *105*, 1103.
(2) Ulman, A. *Chem. Rev.* **1996**, *96*, 1533.
(3) Porter, M. D.; Bright, T. B.; Allara, D. L.; Chidsey, C. E. D. *J. Am. Chem. Soc.* **1987**, *109*, 3559.
(4) Bain, C. D.; Troughton, E. B.; Tao, Y. T.; Evall, J.; Whitesides, G. M.; Nuzzo, R. G. *J. Am. Chem. Soc.* **1989**, *111*, 321.
(5) Shon, Y. S.; Lee, S.; Colorado, R.; Perry, S. S.; Lee, T. R. *J. Am. Chem. Soc.* **2000**, *122*, 7556.
(6) Shon, Y. S.; Lee, S.; Perry, S. S.; Lee, T. R. *J. Am. Chem. Soc.* **2000**, *122*, 1278.
(7) Xiao, X.; Hu, J.; Charych, D. H.; Salmeron, M. *Langmuir* **1996**, *12*, 235.
(8) Lio, A.; Charych, D. H.; Salmeron, M. *J. Phys. Chem. B* **1997**, *101*, 3800.
(9) Lee, S.; Shon, Y. S.; Colorado, R.; Guenard, R. L.; Lee, T. R.; Perry, S. S. *Langmuir* **2000**, *16*, 2220.
(10) Flink, S.; van Veggel, F.; Reinhoudt, D. N. *Adv. Mater.* **2000**, *12*, 1315.
(11) McCreery, R. L.; Bergren, A. J. *Adv. Mater.* **2009**, *21*, 4303.
(12) von Wrochem, F.; Gao, D.; Scholz, F.; Nothofer, H.-G.; Nelles, G.; Wessels, J. M. *Nat. Nanotechnol.* **2010**, *5*, 618.
(13) Nijhuis, C. A.; Reus, W. F.; Siegel, A. C.; Whitesides, G. M. *J. Am. Chem. Soc.* **2011**, *133*, 15397.
(14) Gao, D. Q.; Scholz, F.; Nothofer, H. G.; Ford, W. E.; Scherf, U.; Wessels, J. M.; Yasuda, A.; von Wrochem, F. *J. Am. Chem. Soc.* **2011**, *133*, 5921.
(15) Reus, W. F.; Thuo, M. M.; Shapiro, N. D.; Nijhuis, C. A.; Whitesides, G. M. *ACS Nano* **2012**, *6*, 4806.
(16) Nijhuis, C. A.; Reus, W. F.; Whitesides, G. M. *J. Am. Chem. Soc.* **2010**, *132*, 18386.
(17) Nijhuis, C. A.; Reus, W. F.; Barber, J. R.; Dickey, M. D.; Whitesides, G. M. *Nano Lett.* **2010**, *10*, 3611.
(18) Niljhuis, C. A.; Reus, W. F.; Whitesides, G. M. *J. Am. Chem. Soc.* **2009**, *131*, 17814.
(19) Xing, Y.; Park, T.-H.; Venkatramani, R.; Keinan, S.; Beratan, D. N.; Therien, M. J.; Borguet, E. *J. Am. Chem. Soc.* **2010**, *132*, 7946.
(20) Lee, Y. J.; Jeon, T. C.; Paik, W. K.; Kim, K. *Langmuir* **1996**, *12*, 5830.
(21) Garg, N.; Lee, T. R. *Langmuir* **1998**, *14*, 3815.
(22) Kim, C. H.; Han, S. W.; Ha, T. H.; Kim, K. *Langmuir* **1999**, *15*, 8399.
(23) Lim, J. K.; Kim, Y.; Kwon, O.; Joo, S. W. *Chem. Phys. Chem.* **2008**, *9*, 1781.
(24) Lim, J. K.; Kwon, O.; Joo, S. W. *J. Phys. Chem. C* **2008**, *112*, 6816.
(25) Bruno, G.; Babudri, F.; Operamolla, A.; Bianco, G. V.; Losurdo, M.; Giangregorio, M. M.; Omar, O. H.; Mavelli, F.; Farinola, G. M.; Capezzuto, P.; Naso, F. *Langmuir* **2010**, *26*, 8430.
(26) Srisombat, L. O.; Zhang, S. S.; Lee, T. R. *Langmuir* **2010**, *26*, 41.
(27) Fox, M. A.; Whitesell, J. K.; McKerrow, A. J. *Langmuir* **1998**, *14*, 816.
(28) Kittredge, K. R.; Minton, M. A.; Fox, M. A.; Whitesell, J. K. *Helv. Chim. Acta* **2002**, *85*, 788.
(29) Yam, C. M.; Cho, J.; Cai, C. Z. *Langmuir* **2003**, *19*, 6862.
(30) Park, J. S.; Vo, A. N.; Barriet, D.; Shon, Y. S.; Lee, T. R. *Langmuir* **2005**, *21*, 2902.
(31) Kitagawa, T.; Idomoto, Y.; Matsubara, H.; Hobara, D.; Kakiuchi, T.; Okazaki, T.; Komatsu, K. *J. Org. Chem.* **2006**, *71*, 1362.
(32) Katano, S.; Kim, Y.; Matsubara, H.; Kitagawa, T.; Kawai, M. *J. Am. Chem. Soc.* **2007**, *129*, 2511.
(33) Colorado, R.; Villazana, R. J.; Lee, T. R. *Langmuir* **1998**, *14*, 6337.
(34) Lee, T. C.; Hounihan, D. J.; Colorado, R.; Park, J. S.; Lee, T. R. *J. Phys. Chem. B* **2004**, *108*, 2648.
(35) Lee, T. C.; Chen, P. C.; Lai, T. Y.; Tuntiwechapikul, W.; Kim, J. H.; Lee, T. R. *Appl. Surf. Sci.* **2008**, *254*, 7064.
(36) Moore, H. J.; Colorado, R.; Lee, H. J.; Jamison, A. C.; Lee, T. R. *Langmuir* **2013**, *29*, 10674.
(37) Gothelf, K. V. *J. Electroanal. Chem.* **2000**, *494*, 147.
(38) Zhao, Y.; Perez-Segarra, W.; Shi, Q. C.; Wei, A. *J. Am. Chem. Soc.* **2005**, *127*, 7328.
(39) Morf, P.; Raimondi, F.; Nothofer, H. G.; Schnyder, B.; Yasuda, A.; Wessels, J. M.; Jung, T. A. *Langmuir* **2006**, *22*, 658.
(40) Weinstein, R. D.; Richards, J.; Thai, S. D.; Omiatek, D. M.; Bessel, C. A.; Faulkner, C. J.; Othman, S.; Jennings, G. K. *Langmuir* **2007**, *23*, 2887.
(41) Zhu, H.; Coleman, D. M.; Dehen, C. J.; Geisler, I. M.; Zemlyanov, D.; Chmielewski, J.; Simpson, G. J.; Wei, A. *Langmuir* **2008**, *24*, 8660.
(42) Shon, Y. S.; Lee, T. R. *Langmuir* **1999**, *15*, 1136.
(43) Shon, Y. S.; Lee, T. R. *J. Phys. Chem. B* **2000**, *104*, 8192.
(44) Shon, Y. S.; Colorado, R.; Williams, C. T.; Bain, C. D.; Lee, T. R. *Langmuir* **2000**, *16*, 541.
(45) Park, J. S.; Smith, A. C.; Lee, T. R. *Langmuir* **2004**, *20*, 5829.
(46) Wang, W.; Zhang, S.; Chinwangso, P.; Advincula, R. C.; Lee, T. R. *J. Phys. Chem. C* **2009**, *113*, 3717.
(47) Colorado, R., Jr.; Villazana, R. J. L.; Randall, T. *Langmuir* **1998**, *14*, 6337.
(48) San Juan, R. R.; Carmichael, T. B. *Langmuir* **2012**, *28*, 17701.
(49) Miller, M. S.; Juan, R. R. S.; Ferrato, M.-A.; Carmichael, T. B. *Langmuir* **2011**, *27*, 10019.
(50) San Juan, R. R.; Allan, C. J.; Iqbal, M.; Eichhorn, S. H.; Macdonald, C. L. B.; Carmichael, T. B. *J. Am. Chem. Soc.* **2013**, *135*, 15784.
(51) San Juan, R. R.; Miller, M. S.; Ferrato, M. A.; Carmichael, T. B. *Langmuir* **2012**, *28*, 13253.
(52) Trevor, D. J.; Chidsey, C. E. D.; Loiacono, D. N. *Phys. Rev. Lett.* **1989**, *62*, 929.
(53) Wagner, P.; Hegner, M.; Guntherodt, H. J.; Semenza, G. *Langmuir* **1995**, *11*, 3867.

(54) Weiss, E. A.; Kaufman, G. K.; Kriebel, J. K.; Li, Z.; Schalek, R.; Whitesides, G. M. *Langmuir* **2007**, *23*, 9686.
(55) Naumann, R.; Schiller, S. M.; Giess, F.; Grohe, B.; Hartman, K. B.; Karcher, I.; Koper, I.; Lubben, J.; Vasilev, K.; Knoll, W. *Langmuir* **2003**, *19*, 5435.
(56) Hegner, M.; Wagner, P.; Semenza, G. *Surf. Sci.* **1993**, *291*, 39.
(57) Kumar, A.; Biebuyck, H. A.; Whitesides, G. M. *Langmuir* **1994**, *10*, 1498.
(58) Horcas, I.; Fernandez, R.; Gomez-Rodriguez, J. M.; Colchero, J.; Gomez-Herrero, J.; Baro, A. M. *Rev. Sci. Instrum.* **2007**, *78*, 013705.
(59) Moulder, J. F.; Stickle, W. F.; Sobol, P. E.; Bomben, K. D. *Handbook of X-Ray Photoelectron Spectroscopy*; Perkin-Elmer Corp.: Eden Prairie, MN, 1995.
(60) Castner, D. G.; Hinds, K.; Grainger, D. W. *Langmuir* **1996**, *12*, 5083.
(61) Ishida, T.; Choi, N.; Mizutani, W.; Tokumoto, H.; Kojima, I.; Azehara, H.; Hokari, H.; Akiba, U.; Fujihira, M. *Langmuir* **1999**, *15*, 6799.
(62) Bubert, H.; Jenett, H. *Surface and Thin Film Analysis*; Wiley-VCH: Weinheim, 2002.
(63) Koval, I. V. *Russ. Chem. Rev.* **1994**, *63*, 735.
(64) The distance between adjacent C−P−C planes was calculated assuming a separation distance of 2 Å between the sulfur atoms of nearest neighbor DTPA molecules, and an intramolecular DTPA S−S distance of 3 Å which was calculated for $^{n}Bu_2$DTPA in reference 42.
(65) Ulman, A. *Ultrathin Organic Films*; Academic Press: San Diego, 1991.
(66) Bain, C. D.; Whitesides, G. M. *J. Am. Chem. Soc.* **1989**, *111*, 7164.
(67) Barsoukov, E.; Macdonald, J. R. *Impedance Spectroscopy*, 2nd ed.; Wiley and Sons: Hoboken, NJ, 2005.
(68) Diao, P.; Guo, M.; Tong, R. T. *J. Electroanal. Chem.* **2001**, *495*, 98.
(69) Peterlinz, K. A.; Georgiadis, R. *Langmuir* **1996**, *12*, 4731.